Vertical distribution of ozone on Mars as measured by SPICAM/Mars-Express using stellar occultations

Sébastien Lebonnois, Eric Quémerais, Franck Montmessin, Franck Lefèvre, Séverine Perrier, Jean-Loup Bertaux, François Forget

JOURNAL OF GEOPHYSICAL RESEARCH, VOL. 111, E09S05, doi:10.1029/2005JE002643, 2006

Vertical distribution of ozone on Mars as measured by SPICAM/Mars Express using stellar occultations

Sébastien Lebonnois,[1] Eric Quémerais,[2] Franck Montmessin,[2] Franck Lefèvre,[2] Séverine Perrier,[2] Jean-Loup Bertaux,[2] and François Forget[1]

Received 21 November 2005; revised 16 January 2006; accepted 12 April 2006; published 9 September 2006.

[1] The ultraviolet spectrometer of the SPICAM instrument on board the European Mars Express mission has performed stellar occultations to probe the atmosphere. Vertical profiles of ozone are retrieved from inversion of transmission spectra in the altitude range 20–30 to 70 km. They are analyzed here as functions of latitude and season of the observations. These occultations have been monitored on the night side, from northern spring equinox (L_s = 8°) to northern winter solstice (L_s = 270°). The profiles show the presence of two ozone layers: (1) one located near the surface, the top of which is visible below 30 km altitude, and (2) one layer located in the altitude range 30 to 60 km, a feature that is highly variable with latitude and season. This layer is first seen after L_s = 11°, and the ozone abundance at the peak tends to increase until $L_s \sim 40°$, when it stabilizes around $6–8 \times 10^9$ cm^{-3}. After southern winter solstice ($L_s \sim 100°$), the peak abundance starts decreasing again, and this ozone layer is no longer detected after $L_s \sim 130°$. A recent model (Lefèvre et al., 2004) predicted the presence of these ozone layers, the altitude one being only present at night. Though the agreement between model and observations is quite good, this nocturnal altitude layer is present in SPICAM data over a less extended period than predicted. Though a possible role of heterogeneous chemistry is not excluded, this difference is probably linked to the seasonal evolution of the vertical distribution of water vapor.

Citation: Lebonnois, S., E. Quémerais, F. Montmessin, F. Lefèvre, S. Perrier, J.-L. Bertaux, and F. Forget (2006), Vertical distribution of ozone on Mars as measured by SPICAM/Mars Express using stellar occultations, *J. Geophys. Res.*, *111*, E09S05, doi:10.1029/2005JE002643.

1. Introduction

[2] The SPICAM instrument on board the European Mars Express mission is an ultraviolet and infrared spectrometer working in the ranges [118–300] nm and [1.0–1.7] μm and dedicated to the study of the atmosphere and ionosphere of Mars [*Bertaux et al.*, 2000, 2005, 2006]. The UV channel modes include nadir viewing, limb viewing and vertical profiling of the atmosphere by stellar or solar occultations. The IR channel is dedicated primarily to nadir measurements of the water vapor abundances, vertical profiling of water vapor and aerosols during solar occultations, and detection of 1.27 μm $O_2(^1\Delta_g)$ emissions [*Korablev et al.*, 2002].

[3] Among its scientific objectives, SPICAM can determine and monitor the ozone (O_3) distribution in the atmosphere of Mars. Ozone was detected in the Martian atmosphere by the Mariner 7 (1969) and 9 (1971–1972) ultraviolet spectrometers [*Barth and Hord*, 1971; *Barth et al.*, 1973]. It has since been observed both directly at Mars, including some tentatives of vertical profiling (Mars 5 and Phobos 2 spacecraft [*Krasnopolsky and Parshev*, 1979; *Blamont and Chassefière*, 1993]), and from Earth [*Espenak et al.*, 1991; *Clancy et al.*, 1996, 1999; *Novak et al.*, 2002; *Fast et al.*, 2006]. With its different modes, SPICAM can retrieve atmospheric ozone using three distinct methods: (1) in nadir geometry, the Hartley O_3 absorption band at 250 nm is detected in the solar spectrum scattered back from the ground, that allows the retrieval of the ozone column abundance in the atmosphere; (2) during stellar and solar occultations, the same absorption band is seen in the transmission spectrum, giving access to the ozone abundance along the line of sight, as a function of altitude; (3) in the infrared, the O_2 airglow at 1.27 μm is emitted through relaxation of $O_2(^1\Delta_g)$ excited molecules, which are produced by photodissociation of ozone molecules by solar UV photons, providing an indirect measure of the ozone column above the level below which the $O_2(^1\Delta_g)$ molecules are mostly quenched by CO_2 collisions (approximately 20 km altitude according to models [e.g., *Novak et al.*, 2002]).

[1]Laboratoire de Météorologie Dynamique/IPSL, CNRS/UPMC, Paris, France.
[2]Service d'Aéronomie/IPSL, CNRS/UVSQ/UPMC, Verrières-le-Buisson, France.

0148-0227/06/2005JE002643$09.00

[4] In this paper, we will discuss the second method, using the UV signature of ozone in the transmission spectra that have been obtained during stellar occultations. The SPICAM data set of stellar occultations gives a unique opportunity to understand the vertical distribution of ozone, and its behavior as a function of latitude and season. Up to now, only models have been giving insights into this matter [*Clancy and Nair*, 1996; *Lefèvre et al.*, 2004], though ground-based observations of O_2 airglow at 1.27 μm have also provided some limited information [*Novak et al.*, 2002; *Krasnopolsky*, 2003]. In section 2, we describe the retrieval procedure for the ozone vertical profile, and the distributions of occultations as a function of latitude, longitude, local time and season (i.e., solar longitude L_s). The seasonal and latitudinal evolution of the ozone profiles are discussed (section 3) and compared with the model predictions (section 4), leading to open questions and discussion.

2. Stellar Occultations Data Set

[5] During a stellar occultation, the SPICAM UV field of view is pointed toward a star, and its detector records the stellar spectrum as the spacecraft drifts on its orbit and the star rises or sets behind the atmosphere of Mars. From January 2004 to mid-August 2005, 629 stellar occultations have been observed with SPICAM, among which 433 have been successfully analyzed to retrieve ozone vertical profiles. This set of vertical profiles covers solar longitudes from 8.3° (just after northern spring equinox) to 270° (northern winter solstice). The analysis procedure is described in detail by *Quémerais et al.* [2006], but the essential steps are given in the following section.

2.1. Data Analysis

[6] The method used here is a self-calibrated method, that does not need absolute calibration of the stellar spectra. The wavelength range [120–280] nm is used in order to retrieve CO_2 and O_3 densities along the line of sight (slant densities), as well as aerosols (dust and/or clouds) opacities and spectral behavior [*Montmessin et al.*, 2006]. First, a reference spectrum of the star outside the atmosphere is computed from spectra measured above 180 km altitude, then all spectra during the occultation are ratioed to this reference stellar spectrum, to get atmospheric transmission spectra as a function of the altitude of the tangential point above a reference ellipsoid. For the following study, altitudes provided are given with respect to the MOLA reference ellipsoid.

[7] Wavelengths shortward of 200 nm are used to retrieve CO_2 slant densities, aerosols opacities are affecting the whole spectrum, and longward of 200 nm, the transmission spectra are dominated by CO_2 Rayleigh extinction with an additional trough around 250 nm due to the O_3 absorption band (Figure 1). The depth of this trough is a measure of the ozone slant density, which is then retrieved as a function of altitude. Given the S/N ratio obtained in the stellar occultations analyzed in this paper (around 20; see *Quémerais et al.* [2006] for details), ozone is detected for column densities larger than approximately 10^{15} molecules cm^{-2}, a value that was expected from simulations performed before the mission [*Korablev et al.*, 2001]. Associated error bars are of the order of 1 to 5 × 10^{15} molecules cm^{-2}.

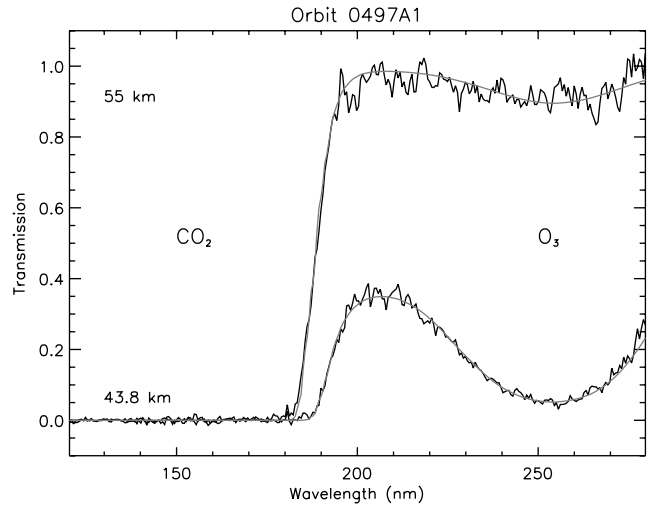

Figure 1. Example of a transmission spectra, for orbit 497A1 (latitude = 29.7°S, longitude = 105.7°E, local time = 21h, solar longitude = 45.5°). Two altitudes are shown: 55.0 and 43.8 km. The calculated fits shown here include the column densities along the line of sight N_{CO_2} and N_{O_3}, and dust parameters: opacity at 250 nm τ and Angström coefficient α ($\tau_{dust} = k\lambda^{-\alpha}$). Values for 55 km altitude are N_{CO_2} = 1.35 × 10^{22} molecules cm^{-2}, N_{O_3} = 9.28 × 10^{15} molecules cm^{-2}, τ = 0., and α = 1., and values for 43.8 km are N_{CO_2} = 4.66 × 10^{22} molecules cm^{-2}, N_{O_3} = 1.93 × 10^{17} molecules cm^{-2}, τ = 0.35, and α = 1.1085.

[8] The vertical profiles of slant column densities of CO_2 and O_3 are then inverted with an "onion peeling" procedure to derive their vertical density profiles. This procedure includes a Tikhonov regularization method to avoid amplification of the noise in the slant densities profiles. This improves the vertical profile, but reduces the vertical resolution, which is typically around 5 km, up to 10 km for the most noisy cases. Depending on the dust opacity, The CO_2 density is retrieved down to the altitude where the stellar signal is lost completely, typically 20–30 km. This characteristic altitude will be called "lowest altitude" hereafter. It depends essentially on the dust opacity above the surface, and also slightly on the star brightness. Dust opacity attenuates the spectral signal on all the SPICAM wavelength range, and the star signal is not detected below this lowest altitude. The dust opacity varies very significantly from one occultation to the other, yielding a large range for lowest altitude values. We use this altitude limit for CO_2 density retrieval as the lower boundary for the ozone density retrieval. The upper boundary for the ozone retrieval procedure is fixed at 80 km altitude, with no signal usually detected above 60–70 km. The detection limit for ozone abundance is approximately 10^8 molecules cm^{-3}, with usual error bars of the order of 10^8 to 10^9 molecules cm^{-3}.

2.2. Distribution of Observations

[9] Figure 2 shows the distribution of the limb tangent coordinates as a function of solar longitude. These coordinates usually do not change significantly as a function of tangent altitude during the duration of the occultation. Longitudes are well sampled at all seasons, but the latitude

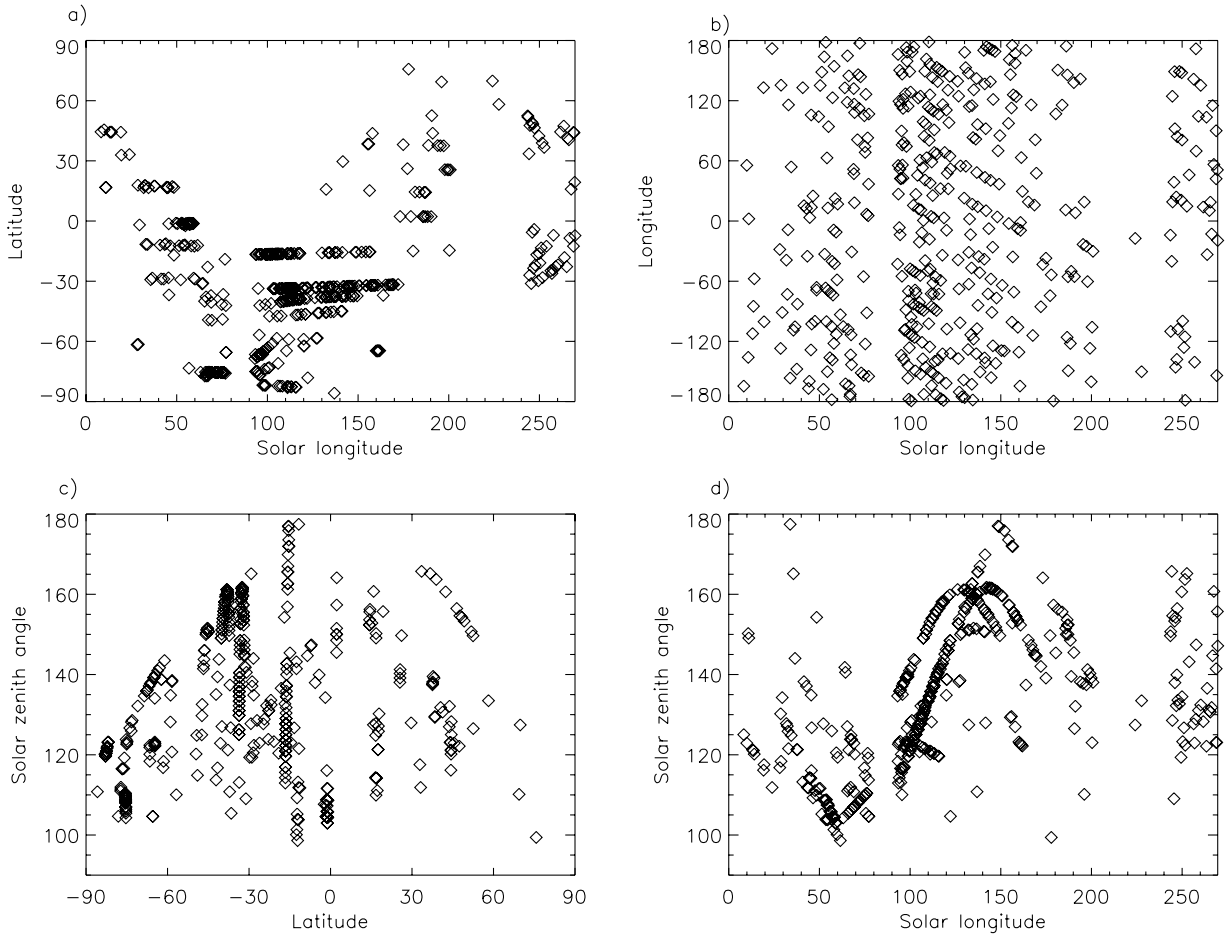

Figure 2. Distributions of the stellar occultations: (a) latitude of the tangential point as a function of solar longitude (i.e., season); (b) same for longitude; and (c and d) solar zenith angle at the tangential point as functions of latitude and season. The uneven sampling is due to a combination of uneven distribution of hot, UV stars in the sky, and Mars Express orbital evolution.

coverage is more restricted. SPICAM is using bright, hot UV stars, which are mainly concentrated near the galactic plane. Coupled with the evolving orbit configuration, this stellar distribution results in an uneven sample of latitudes as a function of season. Therefore Figure 2 indicates that northern latitudes have been sampled mainly before $L_s \sim 50°$ and after $L_s \sim 155°$, while southern latitudes are quite well sampled from $L_s \sim 30°$ to $L_s \sim 155°$, covering most of southern fall and winter seasons.

[10] Occultations are obtained at night with very few exceptions. For daytime occultations, the light reflected by the surface pollutes the signal for low altitudes, resulting in a lowest altitude for retrieval that is very high, typically 60–80 km. Therefore these occultations cannot be used for ozone and are not included in this study. The distributions of solar zenith angles as functions of latitude and season are also shown in Figure 2.

3. Seasonal and Latitudinal Evolution of the Nocturnal Ozone Layer

3.1. Model Prediction of a Nocturnal Ozone Layer

[11] The distribution of ozone was recently studied with a fully three-dimensional General Circulation Model of the Martian atmosphere, that couples dynamics, water cycle, clouds, and atmospheric composition [*Lefèvre et al.*, 2004]. This and all other Mars photochemical models predict that ozone should be present in Mars' atmosphere in places relatively free from HO_x radicals (H, OH, HO_2), which are produced by water photolysis. These places are located above the surface of the winter pole, where water condenses, and at night, above the hygropause; corresponding to two main ozone layers. One layer is located just above the surface, and its abundance is modulated by the atmospheric amount of water vapor near the ground. This ground layer peaks in the dry winter polar regions. The second layer is predicted to appear at night in the middle atmosphere, for altitudes between 25 and 70 km. At these altitudes, ozone is dissociated to $O + O_2$ by ultraviolet photons when the Sun rises, and quickly reformed as ozone ($O + O_2 + M \rightarrow O_3 + M$) after sunset. The magnitude of this nocturnal ozone layer depends on daytime odd oxygen ($O + O_3$) abundances, which are strongly influenced by the amount of water vapor present. Consequently, the nocturnal ozone layer at 20–50 km altitudes is minimized when the hygropause altitude ascends above 40 km altitudes around perihelion season ($L_s \sim 200°$ to $300°$), a modulation mechanism which was first hypothesized by [*Clancy and Nair*, 1996]. This

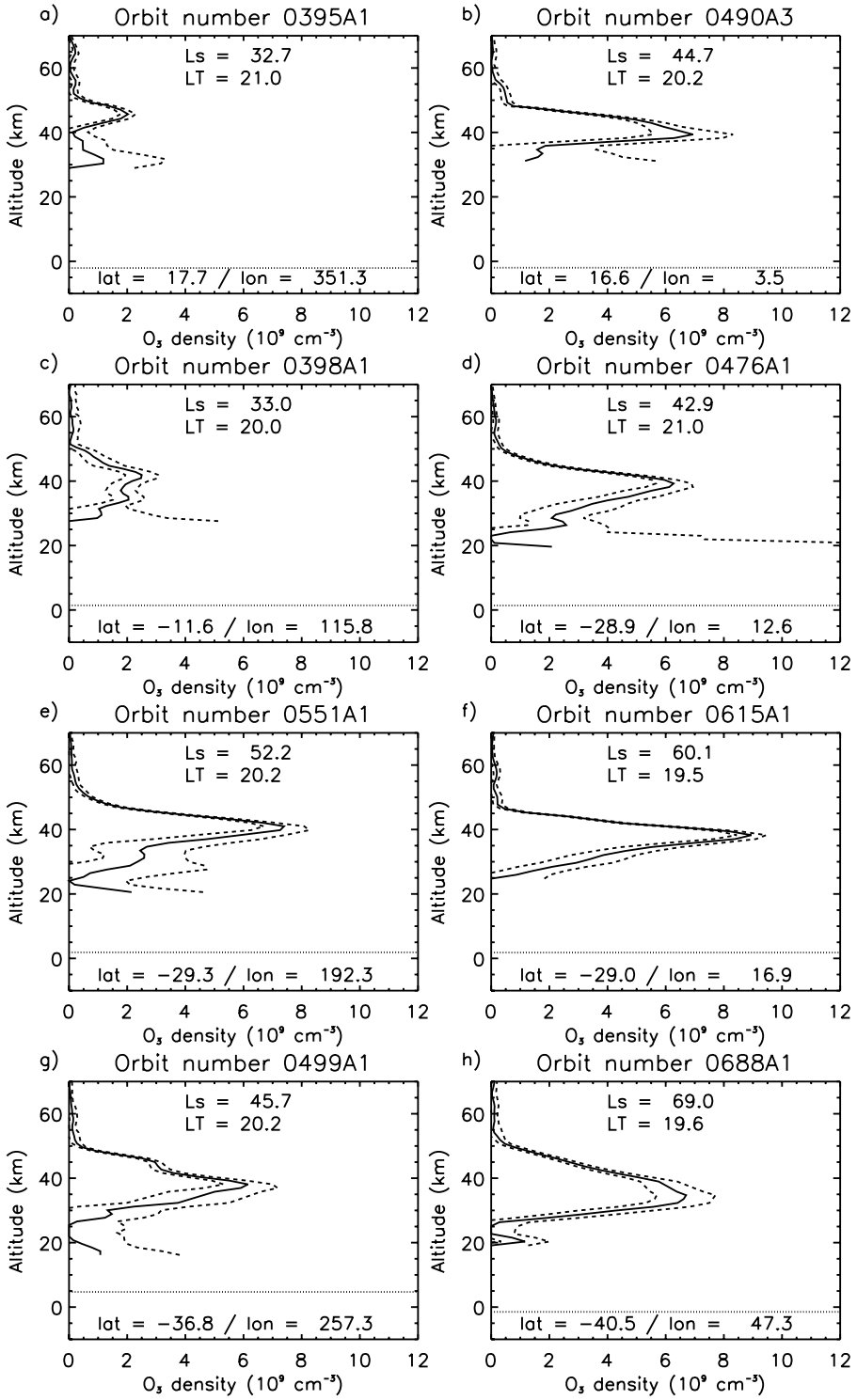

Figure 3. Examples of ozone vertical profiles retrieved for mid and low latitudes during southern autumn (L_s = 8° to 80°), with envelope of uncertainties represented by the dashed curves. Unit is 10^9 cm^{-3}. The origin of the indicated altitudes is the reference surface for MOLA topography. The dotted line shows the position of the surface. (a and b) Latitude range 0–30°N. (c–f) Latitude range 0–30°S. (g and h) Latitude range 30°S–60°S.

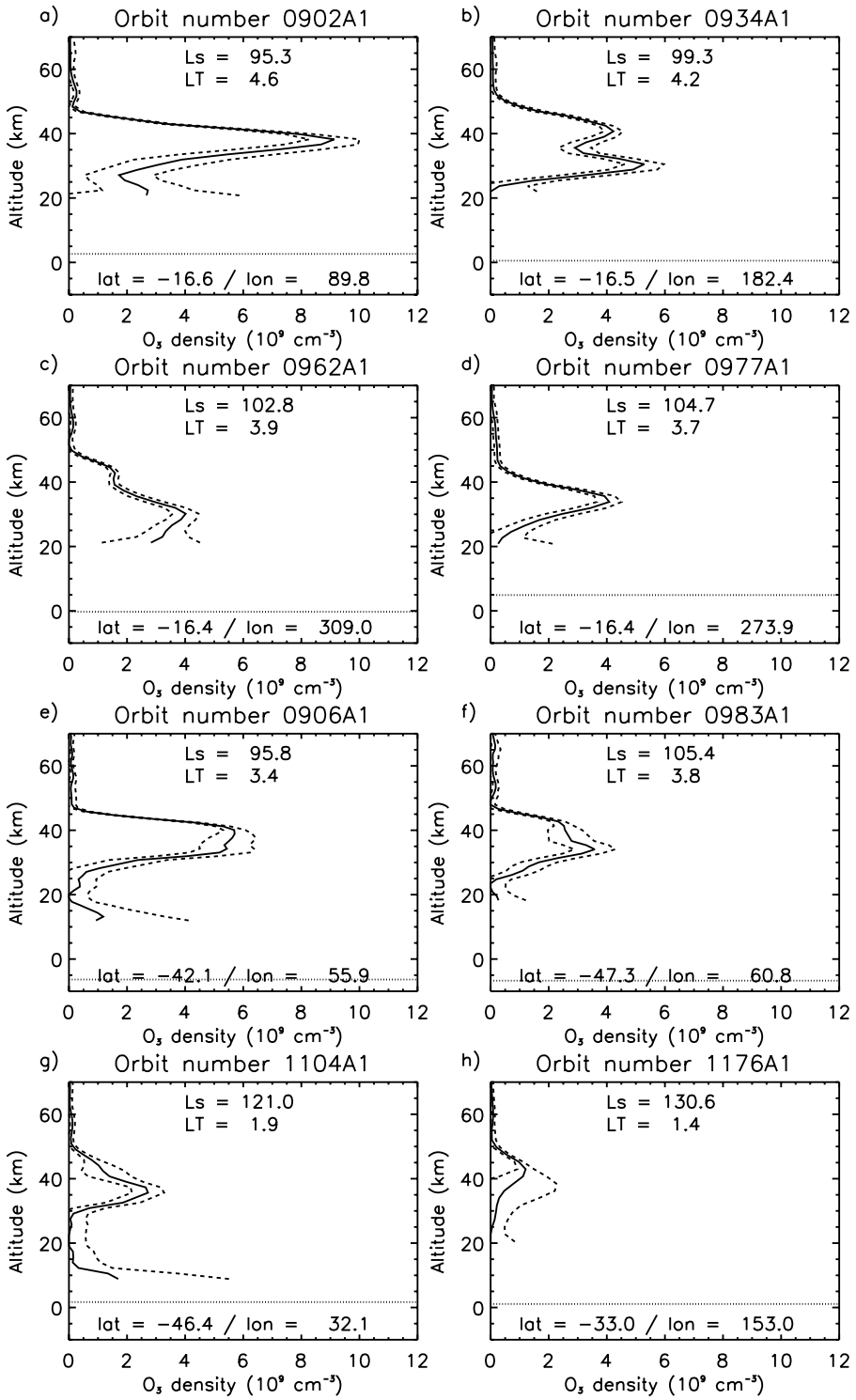

Figure 4. Examples of ozone vertical profiles retrieved for mid and low latitudes during southern winter (L_s = 93° to 155°). (a–d) Latitude range 0–30°S. (e–h) Latitude range 30°S–60°S.

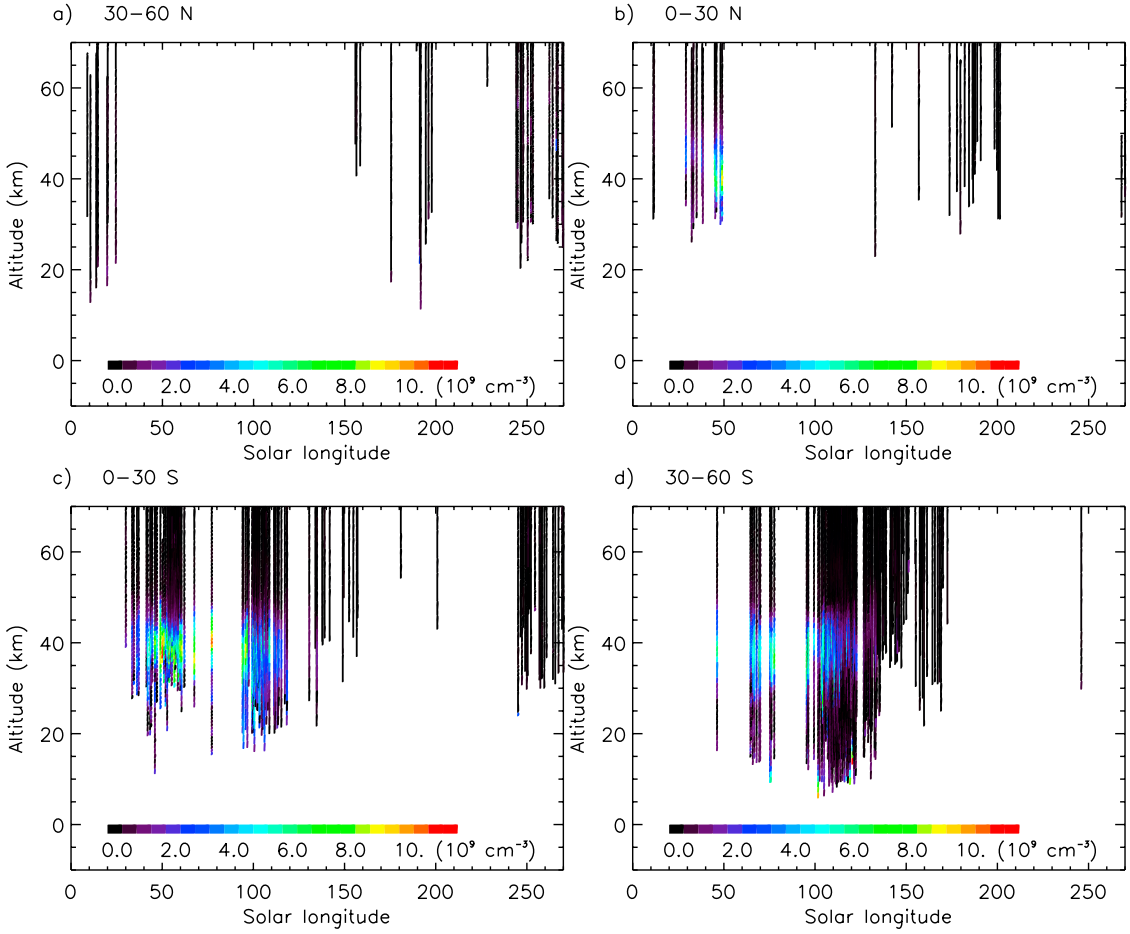

Figure 5. Seasonal evolution of the ozone abundance in the nocturnal layer observed by SPICAM, for different latitude ranges (mid and low latitudes; unit is 10^9 cm^{-3}).

model compared quite well with available data: at L_s = 10° (Figure 9a of *Lefèvre et al.* [2004], with comparison to *Clancy et al.* [1999] observations), and over winter poles (*Barth et al.* [1973] and *Wehrbein et al.* [1979] observations). Around aphelion season though, the model underestimated the equatorial ozone column densities (Figures 9b and 9c of *Lefèvre et al.* [2004]). The vertical profiles obtained here through stellar occultation are an extremely useful tool to test the model predictions, and to better understand the mechanisms controlling composition in this altitude range.

3.2. Mid and Low Latitudes

3.2.1. Southern Autumn

[12] The first stellar occultations monitored by SPICAM, and useful for this study, occurred at L_s = 8° (right after northern spring equinox). SPICAM probed northern mid-latitudes (latitudes between 30 and 60°N) until L_s = 24°. Then, measurements were mostly performed in the tropical region (L_s = 10° to 50° for latitudes between 0 and 30°N, L_s = 30° to 80° for latitudes between 0 and 30°S). During the second half of southern autumn (L_s = 45° to 80°), SPICAM stellar occultations also probed southern mid-latitudes (between 30 and 60°S). Representative profiles for this season and these latitudes are shown in Figure 3.

[13] No ozone is detected during the first occultations, in northern mid-latitudes, though the occultations probed down to roughly 30 km altitude, even down to 20 km in some cases. The upper limit due to error bars is a few 10^8 cm^{-3}. Closer to equator, the lowest altitude of the retrieved profiles is around 35 km altitude. The first ozone layer is detected on orbit 247 (L_s = 11.0°, 2.3°E, 16.8°N), at 52 km altitude, with a peak abundance of (4.7 ± 0.7) × 10^8 cm^{-3}. This peak in ozone density is attributed to the nocturnal ozone altitude layer predicted in the models. For L_s = 28° to 40°, both north and south of the equator, an ozone layer is systematically observed between 35 and 50 km altitude. A peak abundance of 1–4 × 10^9 cm^{-3} is observed in the northern tropics around 45 km altitudes, and of 2–3 × 10^9 cm^{-3} in the southern tropics at slightly lower altitudes. After mid-autumn, the peak altitude tends to be slightly lower, around 40 km, and its abundance increases up to 6–9 × 10^9 cm^{-3}. This is the aphelion season, with apoapsis reach around L_s = 71°. For southern mid-latitudes, the ozone altitude layer is also present during the second half of autumn, with similar characteristics, though its thickness is slightly larger than in the tropics (present between 25–30 and 50 km altitude). Its peak abundance is varying between 4–8 × 10^9 cm^{-3}.

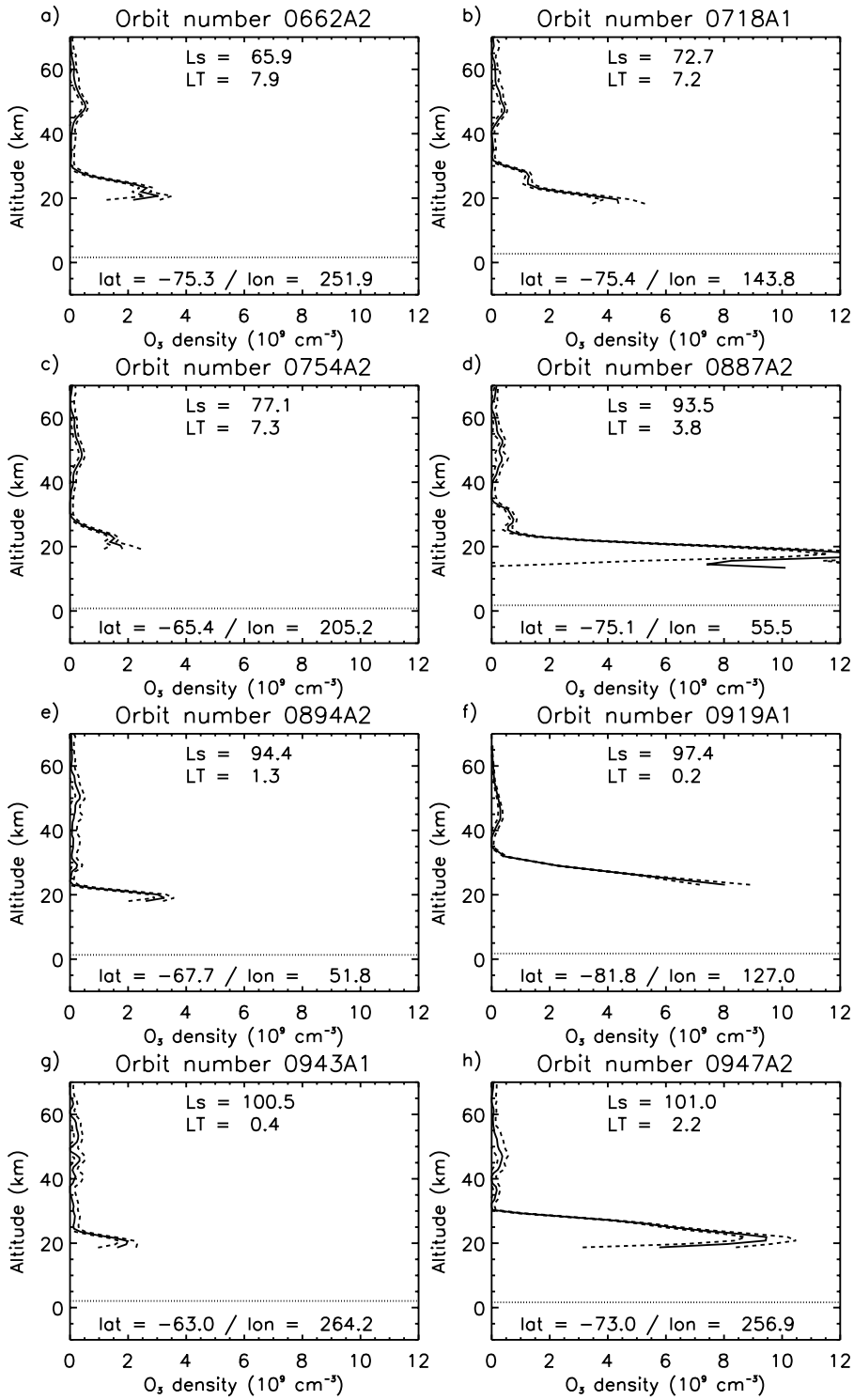

Figure 6. Examples of ozone vertical profiles retrieved for high southern latitudes during southern autumn and winter (L_s = 56° to 160°).

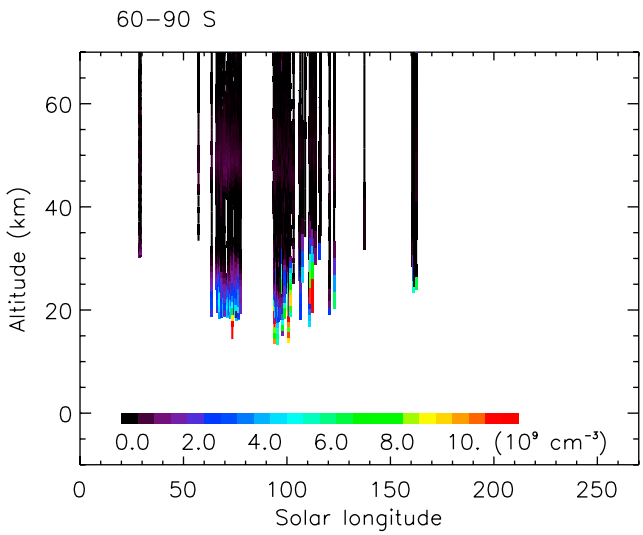

Figure 7. Same as Figure 5, but for southern high latitudes.

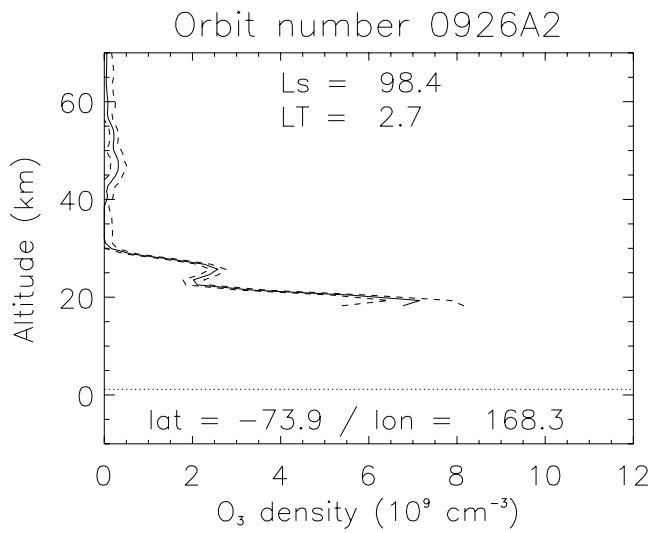

Figure 8. Example of ozone vertical profile showing a structure in the surface layer, with a depletion around 22 km.

3.2.2. Southern Winter

[14] During this season (L_s = 93° to 180°), probed latitudes have been mostly located in the southern hemisphere. Representative profiles for this season and these latitudes are shown in Figure 4.

[15] At low latitudes (0 to 30°S), the occultations probe down to 20–30 km altitude until $L_s \sim 130°$, when the aerosol opacity in the lower atmosphere tends to increase, and the lowest altitude gets higher, around 35–40 km. During early winter (L_s = 93° to 110°), the layer is still thick, between 25 and 45–50 km altitude, with a broad peak around 35–40 km of 5–8 × 10^9 cm^{-3}, decreasing to ~4 × 10^9 cm^{-3} after L_s = 100°. In this layer, double peaks are often observed. After L_s = 110°, ozone is only barely detected on a few orbits, even when the lowest altitude gets down to 30 km.

[16] In mid latitudes (30 to 55°S), this decrease in the ozone altitude layer's abundance with time is also observed. Between L_s = 94° and 122°, the occultations probe very deep, even down to 10 km altitude for many orbits. A broad ozone layer is observed between 30 and 50 km altitude, with a peak abundance decreasing from ~6 × 10^9 cm^{-3} before L_s = 105° to 2–3 × 10^9 cm^{-3} until L_s = 122°. Structures in the layer are seen on a few profiles. Between L_s = 122° and 133°, the ozone altitude layer is still observed between 25 and 50 km altitude, with a peak around 40 ± 5 km, but with lower abundance, less than 2 × 10^9 cm^{-3}. After L_s = 133°, the probing lowest altitude becomes highly variable, located between 30 and 60 km altitude. Similarly to low latitudes, no more ozone is detected at this season.

[17] For latitudes between 55 and 60°S, SPICAM observed 5 occultations. At L_s = 95.5°, a small ozone peak is observed at 30–35 km altitude, with an abundance of 3 × 10^9 cm^{-3}, whereas no ozone is observed in the remaining 4 orbits, even when lowest altitude reaches 20 km.

[18] Many occultations have also been observed at northern latitudes after L_s = 130° (see Figure 2a). Similarly to southern latitudes, the probing lowest altitude is highly variable, and no ozone is detected in the 20 to 70 km region.

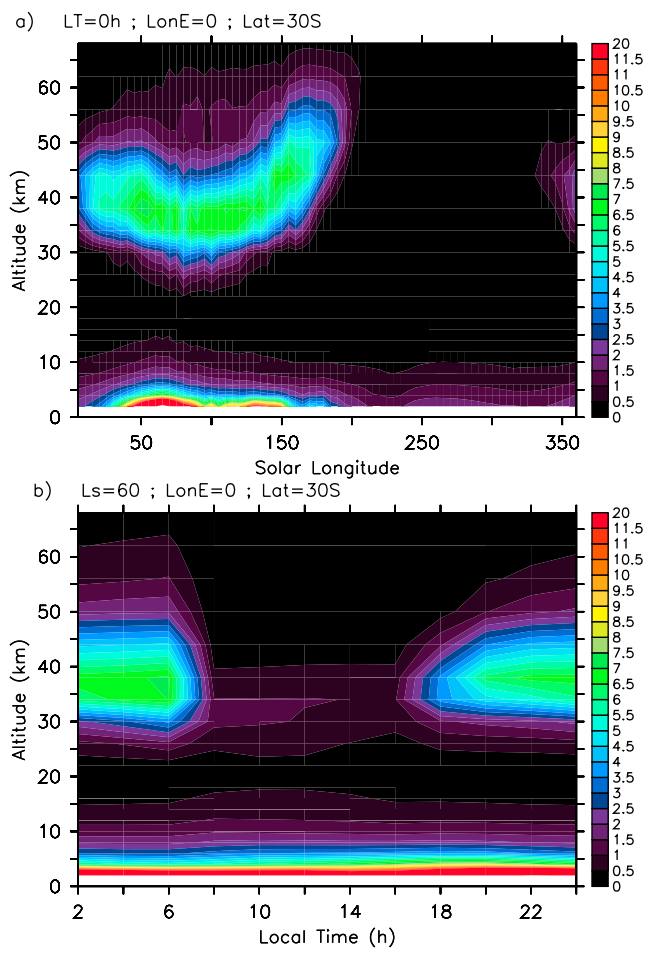

Figure 9. Evolution of the vertical distribution of ozone density (unit is 10^9 cm^{-3}) in the General Circulation Model [*Lefèvre et al.*, 2004] at (0°E, 30°S), as a function of (a) solar longitude (local time is fixed to midnight) and (b) local time (solar longitude is fixed to 60°).

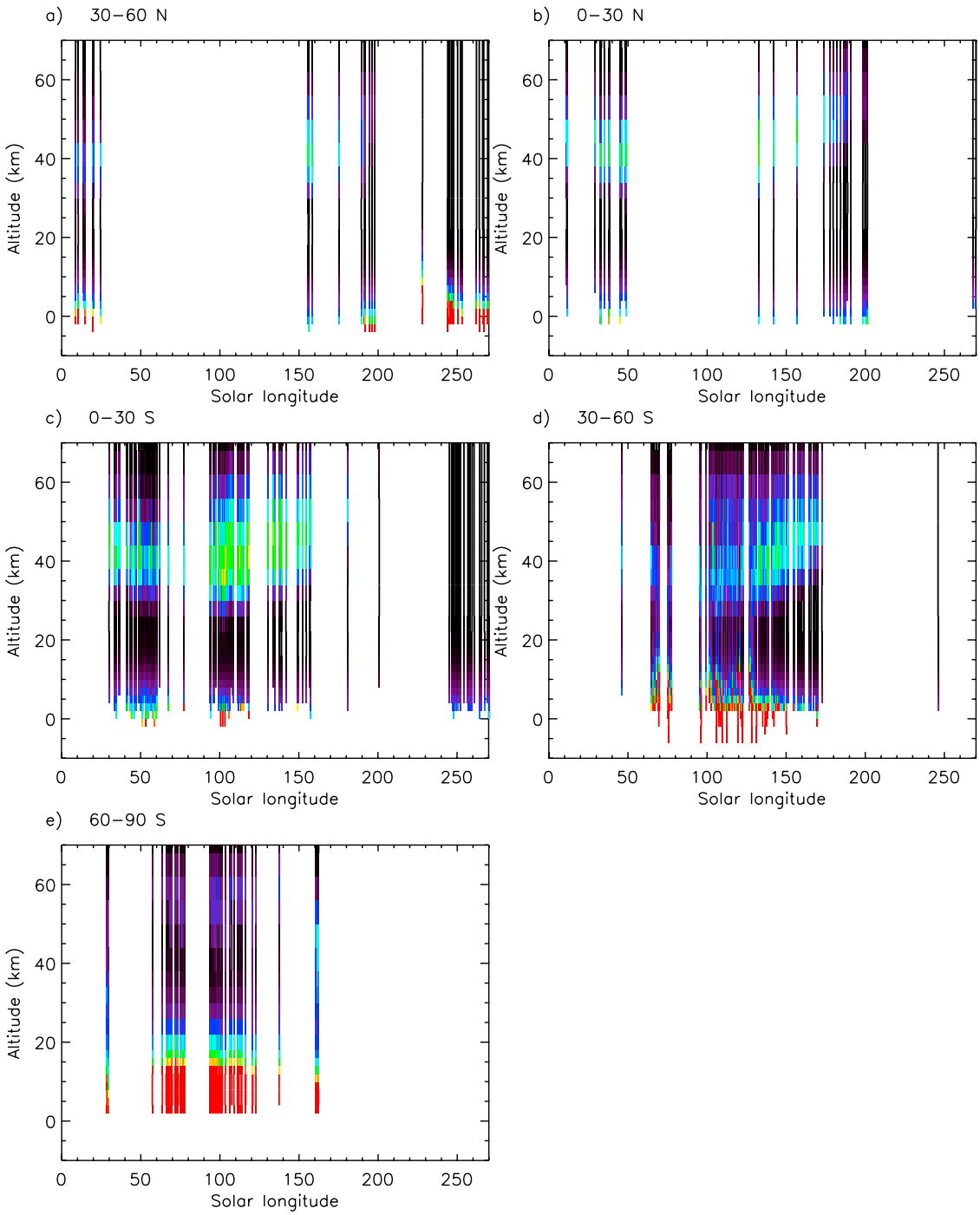

Figure 10. Abundances predicted in the General Circulation Model at the same location and season as observations (Figures 5 and 7), from the surface up to 70 km altitude (unit and color scale are the same as for observed values).

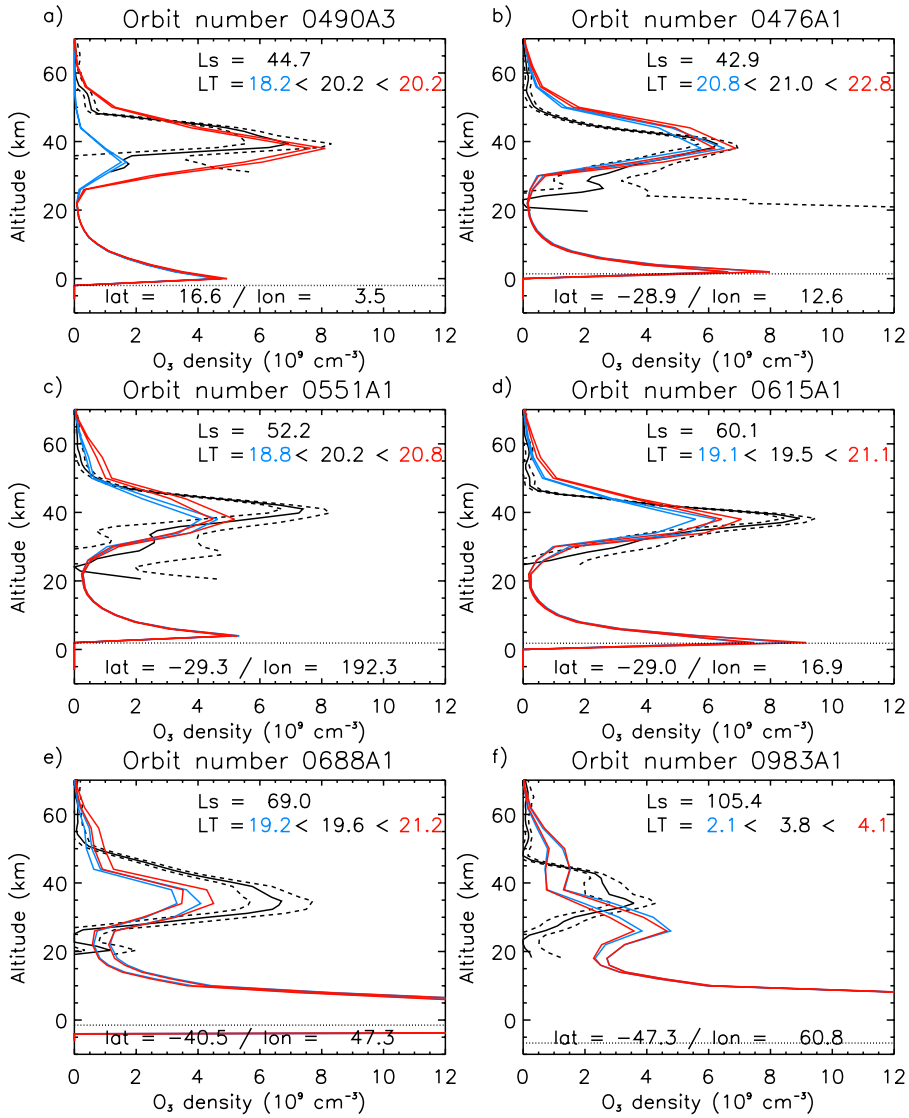

Figure 11. Comparison of observed and modeled ozone vertical profiles for mid and low latitudes, in the period where there is a general agreement ($L_s \sim 40°$ to $L_s \sim 100°$). For the modeled profiles, two local times are shown (output of the model is done every two hours), and for each local time, the two plotted curves show the variability predicted by the model over a period of $\Delta L_s = 5°$ (i.e., mean profile, plus and minus standard deviation). (a) Latitude range 0–30°N. (b–d) Latitude range 0–30°S. (e and f) Latitude range 30°S–60°S.

3.2.3. Northern Fall

[19] Between northern fall equinox and northern winter solstice, occultations have been performed for latitudes ranging from 30°S to 60°N, with only 3 occultations in the northern polar region. Probing lowest altitude varies from 50 to 20 km, but no ozone is detected at this season for any latitude.

[20] Figure 5 summarizes all the vertical profiles of ozone observed for mid and low latitudes. The ozone altitude layer appears essentially between $L_s \sim 40°$ and $L_s \sim 110°$, which is approximately centered on the aphelion ($L_s = 71°$).

3.3. Southern High Latitudes

[21] Latitudes poleward of 60°S have been probed in late autumn and winter, between $L_s = 56°$ and 162°. Most of the profiles present similar characteristics, and representative profiles are shown in Figure 6. The lowest altitude of the profiles is located between 15 and 30 km. A small ozone layer is observed in the altitude range 40 to 60 km, with a peak altitude around 50 km, and an abundance of approximately $2–5 \times 10^8$ cm^{-3} (error bars are approximately 1×10^8 cm^{-3}), before $L_s \sim 125°$. No ozone is detected for the last six occultations, at $L_s = 136°$ and $L_s = 160–161°$, down to 25–30 km altitude. Two additional occultations obtained at $L_s = 28–29°$ and latitude 61.5 detected no ozone down to 35 km altitude, with a noise level around 2×10^8 cm^{-3}. Figure 7 summarizes all the vertical profiles of ozone observed for high-latitudes.

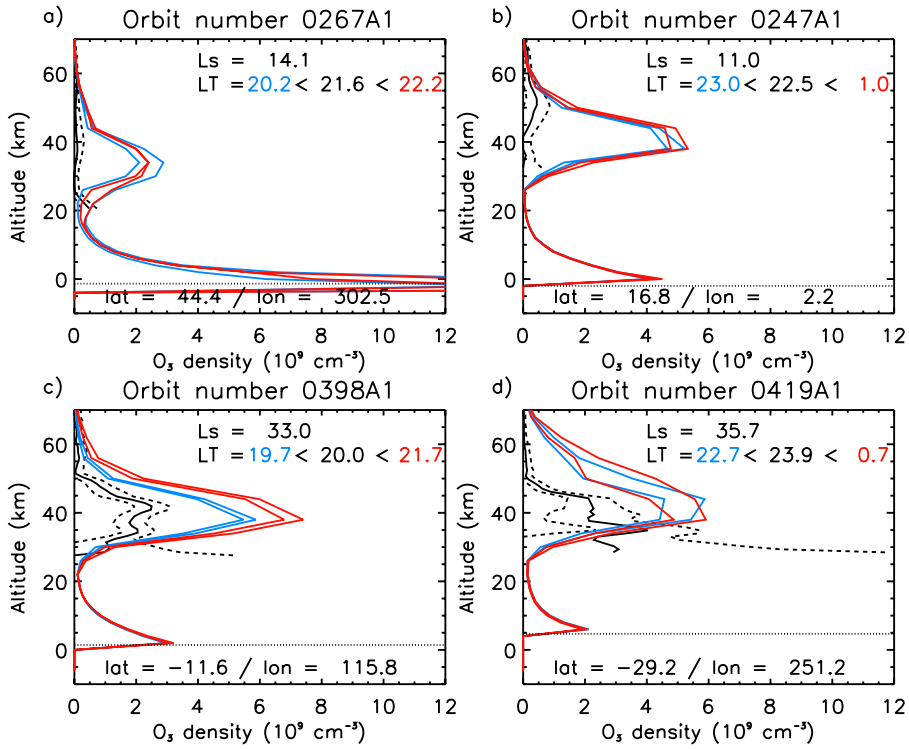

Figure 12. Same as Figure 11, for mid and low latitudes before $L_s \sim 40°$.

[22] At lower altitudes, below 30 km, ozone abundance is increasing with decreasing altitudes. This is consistent with the presence of a surface layer of ozone, detectable over the winter polar region. The atmospheric model [*Lefèvre et al.*, 2004] predicted that the ozone near-surface abundance should be much higher in the winter polar region compared to tropics, due to the depletion in atmospheric water vapor. On one third of the profiles reaching down to 20 km, some structure is visible in this layer, with a depletion of ozone around 20–25 km, as shown in Figure 8.

4. Comparison to Model

4.1. Seasonal Trend, Mid and Low Latitudes

[23] As detailed in section 3.1, a nocturnal ozone layer was predicted by a coupled chemistry-transport 3-dimensional General Circulation Model [*Lefèvre et al.*, 2004] in the altitude range where SPICAM observed it. Figure 9a shows the evolution of this predicted layer at midnight, as a function of solar longitude (mean value over $\Delta L_s = 5°$), for the point (0°E, 30°S). The persistence of the altitude layer over the southern autumn and winter is visible. In order to illustrate the diurnal variations of this ozone layer, Figure 9b shows its evolution as a function of local time, for the same point, and for $L_s = 60°$.

[24] In Figure 10, the abundances predicted in the General Circulation Model are plotted the same way as in Figures 5 and 7, using the same location and solar longitudes. In the period between $L_s \sim 40°$ and $L_s \sim 100–110°$, there is a general agreement between observations and modeled profiles, but the duration of the period during which this nocturnal ozone altitude layer is present is much shorter in the SPICAM data than in the model.

[25] Figure 11 illustrates the agreement between observed and modeled profiles during this period. The thickness of the altitude layer, the peak abundance and the peak altitude are well reproduced by the model in most cases. Figures 12 and 13 show comparisons for $L_s < 40°$ and $L_s > 100°$, respectively, when the modeled profiles do not follow the trends observed at these seasons.

[26] In some cases, double peaks are seen in the observed profiles, as illustrated in Figure 14. Some double peaks are also seen in the model in some profiles, and some similarity can be seen between the observed profile from occultation 0970A1 (Figure 14c) and the modeled profile corresponding to occultation 0975A1 (Figure 14d), for example. The origin of these double peak structures needs further investigations, and the model should help to understand what processes control their occurrence.

4.2. Southern High Latitudes

[27] Poleward of 60°S, during the end of autumn and during winter, the model predicts more ozone in the nocturnal ozone layer than observed (as shown in Figure 15), despite high day-to-day predicted variability. However, the altitude and thickness of this layer are often in good agreement.

[28] Comparison between Figure 7 and Figure 10e indicates that for $L_s \sim 160°$, no ozone is detected while the model predicts the appearance of the nocturnal ozone layer in these conditions. This disagreement is not understood, and will need further investigations.

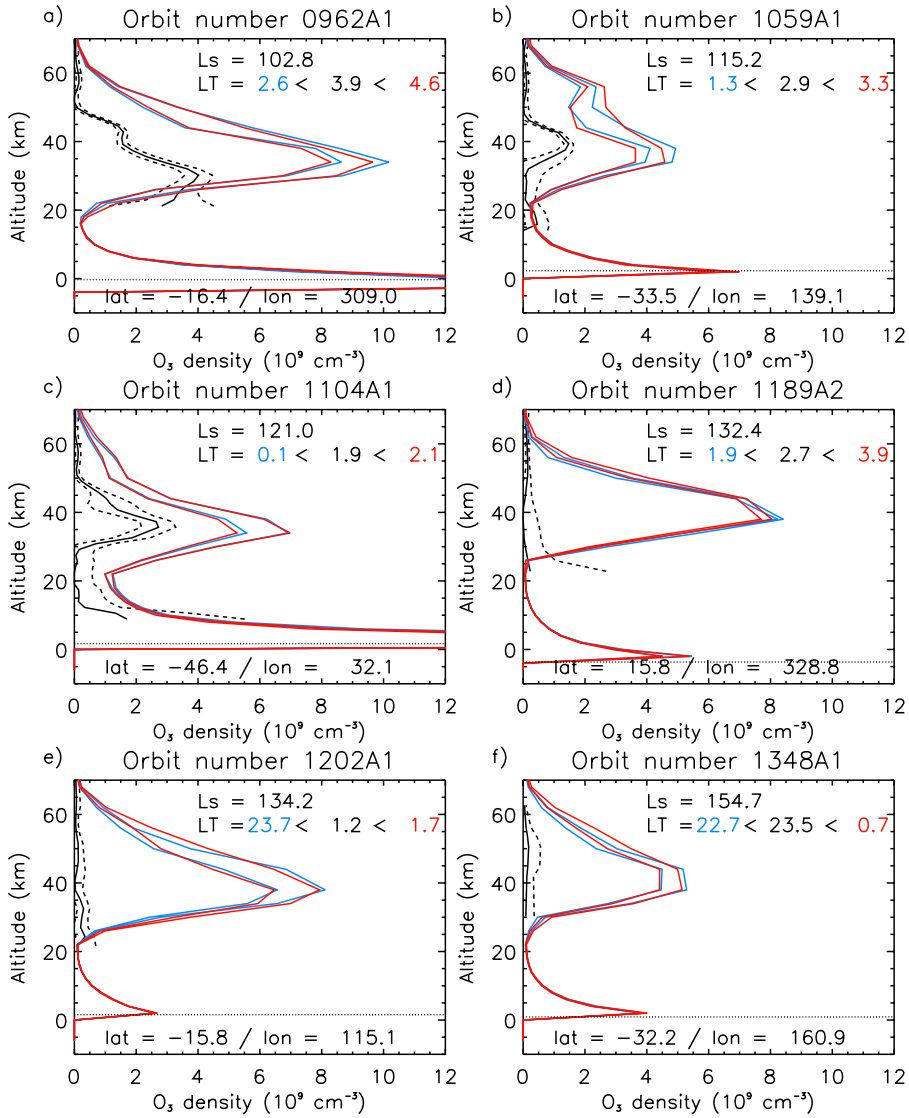

Figure 13. Same as Figure 11, for mid and low latitudes after $L_s \sim 100-110°$.

[29] Below 30 km, the predicted surface ozone layer is mostly in good agreement with the observed profiles, though this layer tends to reach up to higher altitudes for latitudes poleward of 80°S. The model resolution may explain this discrepancy, though higher resolution simulations would be needed to test this hypothesis. As illustrated by occultation 0926A2 (Figure 15d), structures that appear in some observed surface layers, with a depletion around 20–25 km altitude, are never predicted. For some cases, the top of the observed surface layer is largely underestimated by the model, as shown in Figures 15e and 15f.

4.3. Discussion

[30] Several hypothesis may be considered to explain the discrepancy between modeled and observed ozone profiles for altitudes between 30 and 60 km. The observed season for this ozone altitude layer is centered on the aphelion, as in the model, which corresponds to the minimum water vapor content in the atmosphere. Since water vapor plays a key role in the abundance of ozone in this region, through the available amount of HO_x radicals, it seems very likely that a slight shift in the temperature seasonal evolution of this region would induce differences in the water content, and therefore differences in ozone abundance. With the same set of SPICAM stellar occultations, temperature profiles can be retrieved [*Quémerais et al.*, 2006; F. Forget, Temperature and density up to 130 km as measured by SPICAM/Mars Express using stellar occultation, manuscript in preparation, 2006], and compared with the GCM profiles, to see whether observed differences are compatible with this hypothesis.

[31] The infrared channel is not available for stellar occultations, but SPICAM was designed to observe transmission through the atmosphere both in the ultraviolet (retrieving ozone) and in the infrared (retrieving water vapor) during solar occultations. This simultaneous observations of water and ozone profiles, when processing will

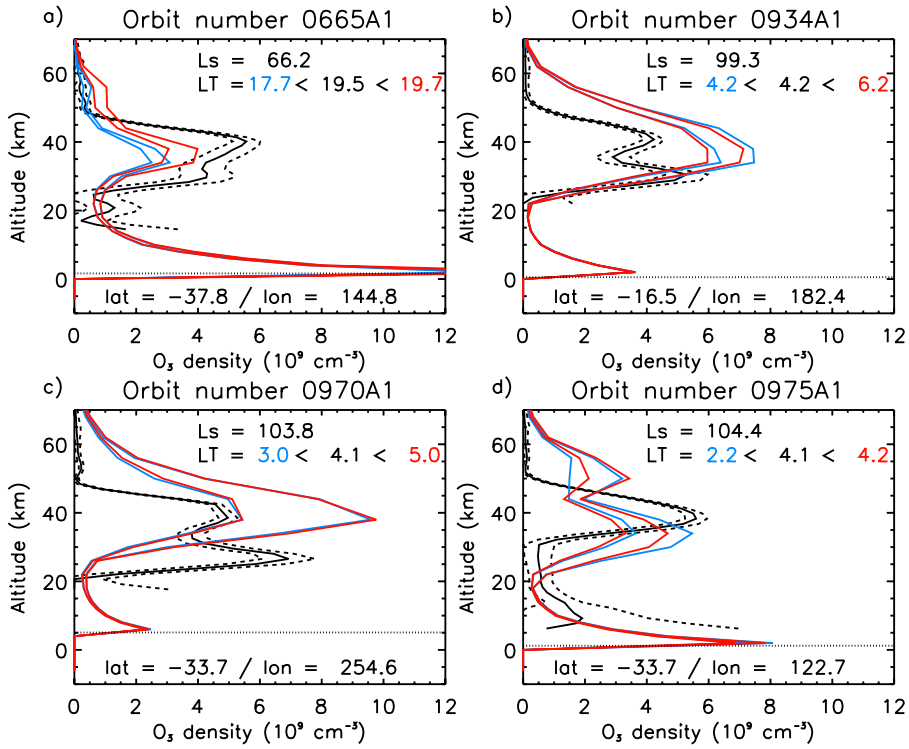

Figure 14. Examples of structures in the nocturnal ozone layer, both in the observed profiles and in the model, for mid and low latitudes.

be completed, should also tell more about the role of water vapor.

[32] There may be possible influences of dust content in this altitude region. It can induce temperature changes, and therefore affect indirectly the water vapor content, and it can also have a direct influence on ozone through potential heterogeneous reactions destroying ozone at the surface of dust particles. SPICAM stellar occultations also enable the monitoring of the dust opacity [*Montmessin et al.*, 2006], but there are very few laboratory data that would help quantify such heterogeneous destruction of ozone.

5. Conclusion

[33] This work describes the vertical profiles of ozone observed by SPICAM/Mars Express, by stellar occultations, during the first Martian year of the mission, from northern spring equinox (L_s = 0°) to northern winter solstice. These observations, done on the night side, cover southern hemisphere during autumn and winter (L_s = 20° to 155°), and latitudes from 30°S to 60°N during northern early spring (L_s < 50°) and autumn (L_s > 155°). Ozone profiles are retrieved between roughly 20 km and 70 km altitude.

[34] A nocturnal ozone layer is observed in the altitude range 30 to 60 km. For mid and low latitudes, its abundance is rising before L_s = 40°, with a peak abundance, around 40 km altitude, of 6–9 × 10^9 cm^{-3} at its maximum, then is decreasing again after L_s ~100°, disappearing completely after L_s ~ 130°. For southern high-latitudes, this layer is barely detected during autumn and early winter, with a peak abundance of 2–5 × 10^8 cm^{-3}, at ~50 km altitude. These observations confirm the predictions of the coupled chemistry-transport General Circulation Model of *Lefèvre et al.* [2004]. The agreement is good in mid and low latitudes, when the observed ozone altitude layer is around its maximum, during aphelion season, but otherwise, the predicted layer tends to be overestimated. The abundance of ozone at these altitudes is controlled by the amount of HO_x radicals, products of water vapor photolysis in this region, and therefore is very dependent on the water vapor vertical distribution. Considering the lack of information on ozone vertical profiles that was available before this SPICAM data set, the good agreement between model predicted profiles and observations is very encouraging, and should help validate our understanding of the ozone chemical cycle in the Martian atmosphere.

[35] When the occultations probe as deep as 20 km altitude, or less, the top of an ozone surface layer is also seen where it is expected, i.e., above winter high-latitudes, where water vapor condenses and ozone may accumulate, protected both from UV photons and from HO_x radicals.

[36] Our understanding of the overall ozone climatology should further improve with more studies to come, combining different SPICAM data sets: with the same set of stellar occultations, temperature and dust opacity profiles are also obtained; solar occultations, that should allow simultaneous retrieval of both ozone and water vapor profiles; dayside nadir observations, that are sensitive to

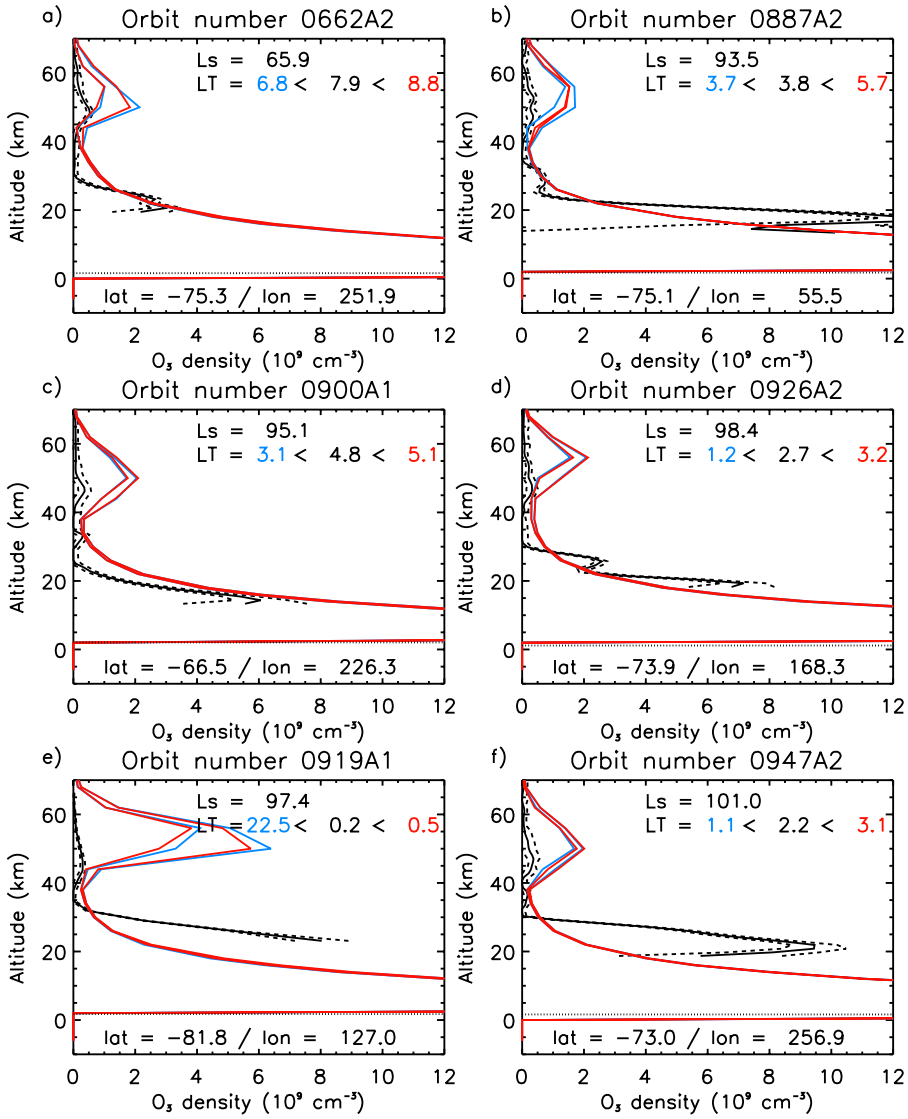

Figure 15. Same as Figure 11, for high latitudes.

the ozone surface layer [*Perrier et al.*, 2006]; and $O_2(^1\Delta_g)$ emissions at 1.27 μm, that give access to the dayside amount of ozone above 20 km altitude.

[37] **Acknowledgments.** Mars Express is a space mission from ESA (European Space Agency). We wish to express our gratitude to all ESA members who participated in this successful mission, and in particular to the ESOC team for the delicate controlling of the spacecraft and Rene Pischel and Tanja Zeghers at ESTEC for careful planning exercises. We thank also Astrium Corp. for the design and construction of the spacecraft and in particular Alain Clochet. We thank our collaborators at the three institutes for the design and fabrication of the instrument (Service d'Aéronomie/France, BIRA/Belgium, and IKI/Moscow) and in particular Emmanuel Dimarellis as Project Manager at Service d'Aéronomie. We wish to thank CNRS and CNES for financing SPICAM in France. We wish to thank the Space Division of the Belgian Federal Science Policy Office for supporting this project through the ESA PRODEX program. The Russian team acknowledges support of RFFI grant 04-02-16856-a.

References

Barth, C. A., and C. W. Hord (1971), Mariner ultraviolet spectrometer: Topography and polar cap, *Science*, *173*(3993), 197–201.

Barth, C. A., C. W. Hord, A. I. Stewart, A. L. Lane, M. L. Duck, and G. P. Anderson (1973), Mariner 9 ultraviolet spectrometer experiment: Seasonal variation of ozone on Mars, *Science*, *179*, 795–796.

Bertaux, J.-L., et al. (2000), The study of the Martian atmosphere from top to bottom with SPICAM light on Mars Express, *Planet. Space Sci.*, *48*(12–14), 1303–1320.

Bertaux, J.-L., et al. (2005), Global structure and composition of the Martian atmosphere with SPICAM on Mars Express, *Adv. Space Res.*, *35*(1), 31–36.

Bertaux, J.-L., et al. (2006), SPICAM on board Mars Express: Instrument, operations, observing modes, and overview of typical results, *J. Geophys. Res.*, doi:10.1029/2006JE002690, in press.

Blamont, J. E., and E. Chassefière (1993), First detection of ozone in the middle atmosphere of Mars from solar occultation measurements, *Icarus*, *104*, 324–336.

Clancy, R. T., and H. Nair (1996), Annual (perihelion-aphelion) cycles in the photochemical behavior of the global Mars atmosphere, *J. Geophys. Res.*, *101*(E5), 12,785–12,790.

Clancy, R. T., A. W. Grossman, M. J. Wolff, P. B. James, Y. N. Billawala, B. J. Sandor, S. W. Lee, and D. J. Rudy (1996), Water vapor saturation at low altitudes around Mars aphelion: A key to Mars climate?, *Icarus*, *122*, 36–62.

Clancy, R. T., M. J. Wolff, and P. B. James (1999), Minimal aerosol loading and global increases in atmospheric ozone during the 1996–1997 Martian northern spring season, *Icarus*, *138*, 49–63.

Espenak, F., M. J. Mumma, T. Kostiuk, and D. Zipoy (1991), Ground-based infrared measurements of the global distribution of ozone in the atmosphere of Mars, *Icarus*, *92*, 252–262.

Fast, K., et al. (2006), Ozone abundance on Mars from infrared heterodyne spectra. I: Acquisition, retrieval, and anticorrelation with water vapor, *Icarus*, *183*, 396–402.

Korablev, O., J.-L. Bertaux, and J.-P. Dubois (2001), Occultation of stars in the UV: Study of the atmosphere of Mars, *J. Geophys. Res.*, *106*(E4), 7597–7610.

Korablev, O., J.-L. Bertaux, A. Grigoriev, E. Dimarellis, Y. Kalinnikov, A. Rodin, C. Muller, and D. Fonteyn (2002), An AOTF-based spectrometer for the studies of Mars atmosphere for Mars-Express mission, *Adv. Space Res.*, *29*(2), 143–150.

Krasnopolsky, V. A. (2003), Mapping of Mars O_2 1.27 μm dayglow at four seasonal points, *Icarus*, *165*, 315–325.

Krasnopolsky, V. A., and V. A. Parshev (1979), Ozone photochemistry of the Martian lower atmosphere, *Planet. Space Sci.*, *27*, 113–120.

Lefèvre, F., S. Lebonnois, F. Montmessin, and F. Forget (2004), Three-dimensional modeling of ozone on Mars, *J. Geophys. Res.*, *109*, E07004, doi:10.1029/2004JE002268.

Montmessin, F., E. Quémerais, J. L. Bertaux, O. Korablev, P. Rannou, and S. Lebonnois (2006), Stellar occultations at UV wavelengths by the SPICAM instrument: Retrieval and analysis of Martian haze profiles, *J. Geophys. Res.*, doi:10.1029/2005JE002662, in press.

Novak, R. E., M. J. Mumma, M. A. DiSanti, N. Dello Russo, and K. Magee-Sauer (2002), Mapping of ozone and water in the atmosphere of Mars near the 1997 aphelion, *Icarus*, *158*, 14–23.

Perrier, S., J. L. Bertaux, F. Lefèvre, S. Lebonnois, O. Korablev, A. Fedorova, and F. Montmessin (2006), Global distribution of total ozone on Mars from SPICAM/MEX UV measurements, *J. Geophys. Res.*, doi:10.1029/2006JE002681, in press.

Quémerais, E., J.-L. Bertaux, O. Korablev, E. Dimarellis, C. Cot, B. R. Sandel, and D. Fussen (2006), Stellar occultations observed by SPICAM on Mars Express, *J. Geophys. Res.*, doi:10.1029/2005JE002604, in press.

Wehrbein, W. M., C. W. Hord, and C. A. Barth (1979), Mariner 9 ultraviolet spectrometer experiment: Vertical distribution of ozone on Mars, *Icarus*, *38*, 288–299.

J.-L. Bertaux, F. Lefèvre, F. Montmessin, S. Perrier, and E. Quémerais, Service d'Aéronomie, IPSL, BP 3, F-91371 Verrières-le-Buisson, France.

F. Forget and S. Lebonnois, Laboratoire de Météorologie Dynamique, IPSL, CNRS/UPMC, Box 99, F-75252 Paris Cedex 05, France. (sebastien.lebonnois@lmd.jussieu.fr)